



CRITICAL ANALYSIS OF SHORELINE LOCALIZATION METHODS BY MEANS OF AERIAL OR SATELLITE IMAGERY ON MEDITERRANEAN SANDY BEACHES

**Giorgio Manno^{*}, Giovanni B. Ferreri^{*}, Gaspare Barbaro^{*}, Antonio Bevilacqua^{*},
Vincenzo Franco^{*}, Giuseppe Mallandrino^{*}, Pietro Orlando^{*}, Vincenzo Ruisi^{*}, Benedetto
Villa^{*}, Marianna Zito^{*}**

^{*} Dipartimento di Ingegneria Civile, Ambientale, Aerospaziale, dei Materiali (DICAM)
Università degli Studi di Palermo
Viale delle Scienze, 90128 Palermo, Italy
e-mail: giovannibattista.ferreri@unipa.it – Tel.: +39 091 238 96572

(Ricevuto 7 Febbraio 2012, Accettato 10 Marzo 2013)

Key words: Shoreline localization; sandy beaches; run-up; tides; aerial imagery.

Parole chiave: linea di riva, spiagge sabbiose, run-up, immagini aeree.

Abstract. *Shoreline localization is fundamental for designing and planning shore protection works as well as for managing and monitoring various anthropic activities along the coast. The sea-land boundary, however, changes continually with time because of waves and tides, which makes the shoreline detection complex and dubious and the boundary line finally assumed can only be conventional. In the last few decades the use of several geomorphologic indicators has been proposed, such as the berm above sea level, the groundwater exit point, historic high tide levels, etc., but the aim has not been achieved yet. Among the methods used, analysis of aerial and satellite imagery is common, in particular when historic evolution of the coast has to be reconstructed. However, the land-sea boundary obtained by images is just one of the countless instantaneous boundaries, which is determined by the particular position of the sea surface and beach geomorphology at the time when images are taken. In this paper a multidisciplinary method is used to estimate the uncertainties caused by wave motion and tides on the shoreline position assessed by aerial or satellite imagery. The method is applied to a beach of the Mediterranean Sea in geomorphologic equilibrium, on the west coast of Sicily. The method explicitly takes into account various physical aspects of the coastal stretch studied and can be adopted for other analogous beaches.*

Sommario. *La localizzazione della linea di riva è fondamentale per sia per progettare e pianificare le opere di difesa della costa sia per gestire e monitorare le molteplici attività antropiche lungo la costa. Il confine terra-mare, tuttavia, muta continuamente nel tempo a causa delle onde e delle maree, il che ne rende complessa e incerta la localizzazione, e la linea infine assunta può essere solo convenzionale. Negli ultimi decenni è stato proposto l'impiego di alcuni indicatori geomorfologici, come la berma di spiaggia emersa, la linea di risorgenza, il livello storico di alta marea, ecc., ma il problema non è ancora risolto. Fra i metodi utilizzati, vi è l'analisi di immagini aeree o da satellite, in particolare quando si voglia ricostruire l'evoluzione storica di un litorale. Tuttavia, il confine terra-mare acquisito da un'immagine aerea è uno degli infiniti confini istantanei, determinato dalla particolare posizione della superficie marina e dalla conformazione geomorfologica della spiaggia proprio nell'istante della ripresa. In questo lavoro si utilizza un metodo multidisciplinare per valutare le incertezze causate dal moto ondoso e dalle maree sulla posizione della linea di riva valutata sulla base di immagini aeree o da satellite. Il metodo è applicato ad una spiaggia in equilibrio geomorfologico del Mar Mediterraneo, situata sulla costa occidentale della Sicilia. Il metodo prende in considerazione espressamente vari aspetti fisici del tratto di costa studiato e può essere utilizzato per altre spiagge analoghe.*

1 INTRODUCTION

A beach is the element of major economic importance of a coastal system but it is also the most fragile one and the most subject to morphologic changes. Studying beach evolution is fundamental for correct management of a coast, along which urban settlements and economic activities are often built up. However, like every terrestrial landscape element, coastal areas are physical entities in continuous evolution, being modelled by natural forces which, acting at different time scales, determine their evolutionary dynamics both in the short and in the long term. The boundary line between land and sea we distinguish in all the topographic and nautical maps and having legal significance is called *shoreline* (Coastal Engineering Manual, 2008). Analysis of shoreline evolution (advancing and retreating) is, in turn, of basic importance for a broad range of investigations involving researchers, technicians, local administrators and managers (Douglas and Crowell, 2000). For instance, shoreline evolution is required for designing coastal protection works (Coastal Engineering Manual, 2008), for coast monitoring (Smith and Jackson 1992), for calibration and validation of numerical models (Hanson and Kraus, 1989), for assessment of sea level rises over millennia (Leatherman, 2001), for assessment of coast erosion (Seymour *et al.*, 2005), for locating risk areas and for recognizing state property and distinguishing it from private property (Morton and Speed, 1998). In addition, to realize the beach's evolutionary trend (Komar, 1998), shoreline location assessment over the years allows one to predict sediment volumes and beach widths (Smith and Jackson, 1992).

Although, from a conceptual point of view, the definition of the shoreline as the "steady" reference boundary between land and sea is rather clear, the never-ending and considerable time variability of the *instantaneous* boundary line in practice makes shoreline determination very difficult. Therefore, some criteria have to be defined on the basis of which *to choose* which of the *countless instantaneous positions* of the land-sea boundary line we can assume as the shoreline. However, the necessity of establishing choice criteria makes us aware that the shoreline assumed will be just a "conventional" land-sea boundary, useful, for example, for settling law controversies or defining damage in the case of floods, its actual physical meaning arising from the particular criteria adopted.

The different criteria for conventionally assuming one shoreline or another, each with sound reasons, may create confusion. For example, U.S.A. rules provide that the shoreline corresponds to the *mean of all the high tides* observed (MHW - Mean High Water). According to this criterion the *instantaneous* land-sea boundary has a noticeably higher probability of being below the *conventional* shoreline than of being above it. By contrast, in other countries, like for instance Italy, the shoreline corresponds to the *mean sea level* observed. In such cases, the probabilities that the instantaneous land-sea boundary will be above or below the conventional boundary are analogous. These considerable differences mirror the fact that, in the present state of things, unambiguous techniques for localizing the shoreline have not been developed. This leads inevitably to major disagreement among experts in the sector such as engineers, geomorphologists and environment managers (May *et al.*, 1982; Dolan *et al.*, 1980).

In spite of the different legal definitions, in practice the custom has been widespread, for many decades, of drawing the shoreline on the basis of aerial images, which allows wide coastal areas to be photographed with relative simplicity and considerably less cost than traditional topographic surveys. However, aerial images have the big drawback of inevitably fixing the land-sea boundary *at the time of shooting*. The instantaneous boundary, of course, arises not only from the particular beach morphology, changeable during each sea storm, but also from the tide level and the run-up or run-down just at the time of shooting. Therefore,

without this information, it is not possible to attribute to the instantaneous land-sea boundary fixed in the images the meaning of a shoreline, whichever rule is in force in the country. The influence of wave motion on the shoreline localization is discussed, among others, by Ruggiero *et al.* (2001). The question then arises of *which sea storm* has to be considered in order to assess the possible shifting of the instantaneous boundary seen in the images from the shoreline we have to determine according to the fixed criteria. As aerial shooting usually is not made in adverse weather conditions, we expect the waves to be within the *normality* of the site considered. In the present paper we assume as the *heaviest normal storm* that having a 1-year return period and, consequently, we also assume the shift between the land-sea boundary shown by the images and the shoreline to be, at most, that estimated using the 1-year sea storm. The latter can be considered as a meteorological-marine *characteristic* of the site.

Use of aerial images is widely employed in studying littoral evolution, as it easily allows one to recognize, with the uncertainties highlighted above, the shoreline advancing and retreating. One of the first and most widely used methods for studying shoreline evolution is aerial image analysis with the help of a stereoscope (Boak and Turner, 2005). Nowadays, with improvement in the available technologies, stereoscopic images can even be used for measuring parameters such as wave length and height in the breaking region (De Vries *et al.*, 2011). Recent image digital processing techniques allow accurate location of the instantaneous land-sea boundary. Noticeable improvement has arisen from georeference techniques (Shoshany and Degani, 1992) as well as from new methods for drawing the dry-wet boundary (Zarillo *et al.*, 2008). Moreover, many remote sensing methods using images at different wave lengths have been developed (Andr  fou  t *et al.*, 2003). For example, near infra-red and thermal infra-red images can be very useful for dividing beach above sea level from submerged beach, although they have a limit in low spatial resolution; by contrast, optical images present better resolution but the often allow poor precision in locating the land-sea boundary, because of foam due to breakers or the presence of submerged vegetation. Among the most widely used remote sensing techniques the following have to be mentioned: radar images (SAR, Synthetic Aperture Radar), Airborne Laser Scanning (LIDAR), wide and narrow band satellite images, etc.. SAR images are taken with a constant period, which makes them very useful for evolution study, although they are sometimes taken in adverse meteorological conditions. It has to be noted that sea waves noticeably affect radar wave reflection (Lee and Jurkevich, 1990). According to Baghdadi *et al.* (2004), radar images are more suitable for locating the land-sea boundary if they are taken with a wide angle of incidence.

LIDAR is another survey method based on beach scanning by a laser telemeter carried by an airplane or an helicopter. The method is particularly suited for simultaneously surveying beach above and below sea level in shallow waters. This technique uses two laser impulses having different wave lengths, one in the green field and the other in the infrared field. The former penetrates through water while the latter is reflected by the sea surface and the beach below sea level. The water depth is obtained by the lag between the signals reflected by the sea surface and the sea bottom (Liu *et al.*, 2007). There also exist methods integrating complementary types of information such as multispectral and geometrical data, thus overcoming the limits of each of the two methods (Lee and Shan, 2003; Deronde *et al.*, 2006).

In order to recognize coastal retreat in a region of Ghana, Addo *et al.* (2008) applied a linear regression to the cartographic data related to the period 1904-2002. The authors, associating with this study the use of mathematical models and geometrical analyses, predicted near coast evolution.

In order to set up correct integrated management of an Indian coastal stretch about 113 km long, Maiti e Bhattacharya (2009) proposed a technique processing data taken from maps and satellite images related to many years. Once the shoreline had been localized in the maps and the imager (for the images the instantaneous land-sea boundary was actually localized), the authors divided the coast into transects and for each of them they statistically analysed the changes in the land-sea boundary. Finally, they formulated predictions on coastal evolution. For sustainable coast management, Valpreda and Simeoni (2003) assumed the shoreline as a morphologic indicator for assessing the coastal risk in a study case (risk due, for example, to beach erosion, flood, storm surge, etc.). The authors deduced the coastal evolution trend just from map indications.

Chen and Chang (2009) studied the changes in the Taiwan west coast shoreline using satellite images (1996-2003) considering tide fluctuations. For better accuracy, the authors compared the instantaneous land-sea boundaries shown by the images with a reference line obtained by GPS RTK survey. The tide effect on the instantaneous boundary was considered by a one-line model (Komar, 1998). Parker (2003) discussed a number of factors which may prejudice correct shoreline location and proposed a technique for better location. The method consists in data acquisition by LIDAR technique, georeference of data with the GPS-RTK system and, finally, a transformation for referring them to MHW with the tool known as NOS's VDatum. Seymour *et al.* (2005) set up a monitoring method for a south California beach using the GPS-RTK technique, and observed that during a 3 m sea wave storm about 160,000 m³ of sediments collected, causing noticeable shoreline movements.

Archetti and Romagnoli (2011) studied the changes in an Italian beach, defended by groynes and a submerged breakwater, during sea storms occurring in a 5 year period. The authors used a video monitoring system (ARGUS) integrated with bathymetric data of the intertidal zone. The authors assumed as a geoinicator the instantaneous land-sea boundary, whose fluctuations were analysed in connection with the waves coming from different directions of exposure.

In conclusion, despite the simple conceptual definition of the shoreline a number of practical difficulties arise for its location, due to the considerable time variability of the land-sea interface which changes continually because of the effects of tides, wave motion and beach remodelling. Consequently, many techniques have been proposed for shoreline location, each with some advantages but also some shortcomings with respect to the others. However, more and more frequent use of aerial and satellite images is observed which, on the one hand, fix the "objective" land-sea boundary at the moment of shooting but, on the other hand, need suitable correction to account for the factors which continually change this boundary. It has to be highlighted that the shoreline established by *images only* is usually assumed as the land-sea boundary of *the whole year* in which the images were taken and it is used for recognizing the coastal evolution trend in years. In the present paper, an interdisciplinary method is proposed for assessing the uncertainties related to tide and wave fluctuations in locating the shoreline on the basis of images only. The method is applied to a study case of a steady sandy beach in west Sicily (Italy).

2 THE METHOD APPLIED

The method applied to assess the uncertainties on the shoreline location starting from aerial images provides for a preliminary geomorphologic study integrated with a hydraulic-maritime study for estimating fluctuations in the instantaneous land-sea boundary due to wave and tide. The effects of currents and sediment transport are neglected here but they will be considered

in further studies. In the present section the method is only described whereas its application will be carried out in the next sections.

The geomorphologic study was performed for the study beach through field observations which allowed us to describe the beach above and below sea level, recognizing the characteristic beach morphotypes, determining sediment size and composition and as surveying several beach transects. The transects were surveyed by a differential GPS technique (RTK - Real Time Kinematic), made possible by the absence of obstacles such as trees, buildings, etc., which might screen the signal. The efficiency of this technique allowed sampling at time intervals of 5 s only, with an error magnitude of 0.02-0.08 m. Bathymetry was obtained by a nautical map and measurements provided by the *Istituto Idrografico della Marina Militare Italiana* (Hydrographic Institute of the Italian Navy). The sediment analysis allowed the topographic survey slopes to be compared with those usually indicated in the literature for the granulometric data collected.

The hydraulic study, aiming at the tide and wave motion effects only, started from identification of the direction of exposure of the coastal waters and from wind analysis, which allowed their preferential direction and intensity to be recognized. For the wave effects an *ordinary* sea storm was considered. In order to estimate the characteristic parameters of such a sea storm we used data provided by the *Istituto Superiore per la Protezione e la Ricerca Ambientale* (ISPRA - Institute for Environmental Protection and Research of the Italian Government, www.idromare.it) recorded by the buoy of the Italian Wavemeter Network which was nearest to the beach. The data were shifted around the area off the beach and then used for the statistical analysis of extreme events. The analysis was performed both directly considering the wave heights measured and, for a comparison, using the *equivalent triangular storm* concept (Boccotti, 2000), which presents the advantage of simplifying sea storm description and statistical analysis of sea storm characteristics. As the offshore wave characteristics were known, the latter were propagated from deep to shallow water using the well-known model SWAN (Simulating Waves Nearshore) for the spectral propagation of wave motion (Boij *et al.* 1999, Holhijsen *et al.* 1993, Ris *et al.* 1999). The nearshore waves were then used for estimating run-up and run-down.

Tide effects were taken into account considering the maximum yearly fluctuations in astronomic and meteorological tide, assessed by processing recordings of the marigraph nearest to the beach. Finally, the data thus produced allowed us to determine a beach strip, around the land-sea boundary fixed by the images, within which all the countless instantaneous boundary lines produced by the ordinary storms fall. In this strip, therefore, the shoreline *has to fall*.

3 BEACH CHARACTERISTICS AND GEOMORPHOLOGY

The beach chosen for application of the method does not present noticeable sediment unbalance and hence its bathymetry remains practically unchanged in time. This beach, moreover, is subject to few human activities (Fig. 1) and therefore it is a practical case in which it is of major importance to succeed in localizing the shoreline or, even better, the extreme fluctuations in the land-sea boundary line, with the aim of defining hazard expectation and state property. Finally, the beach is rather close to a wavemeter buoy.

The beach is known as *Lido Signorino* and is located in western Sicily (Fig. 2); from the geomorphologic viewpoint it falls within the Sicilian physiographic unit N. 14. The Lido Signorino beach has a mild slope, between 1.5 and 10.8°, and is therefore dissipative; it extends in the N-S direction, for about 3.5 km, between the two headlands called Torre Tunna

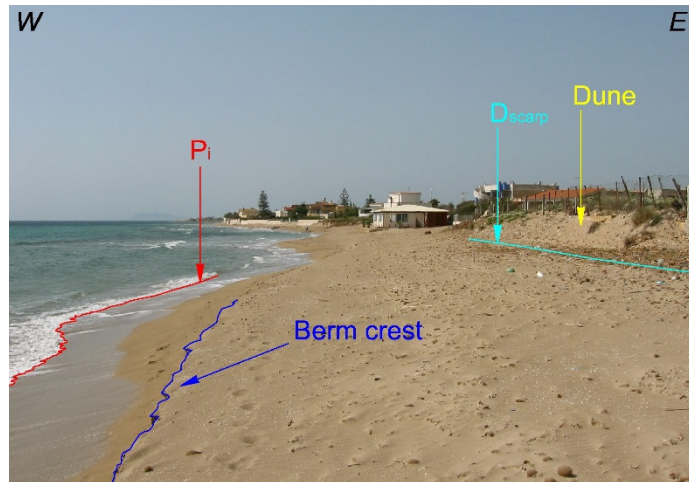


Fig. 1: Lido Signorino beach adopted as study case; the photo shows the berm, the dune and an instantaneous position of the land-sea boundary (P_i).

(325°N - 37°45'32.26"N; 12°27'40.00"E) and Torre Sibilliana (185°N - 37°43'36.31"N; 12°28'11.23"E). The direction of exposure has an amplitude of 140°. Note that, because of the presence of the Egadi archipelago, the beach is screened marginally by the Favignana Island, located along the 320°N direction. The geographic fetch, drawn from the Mediterranean Sea chart with a 1:2,250,000 scale and a 5° angular step, is bounded by the Spanish coast (W), African coast (S) and the Island of Sardinia (N-W).

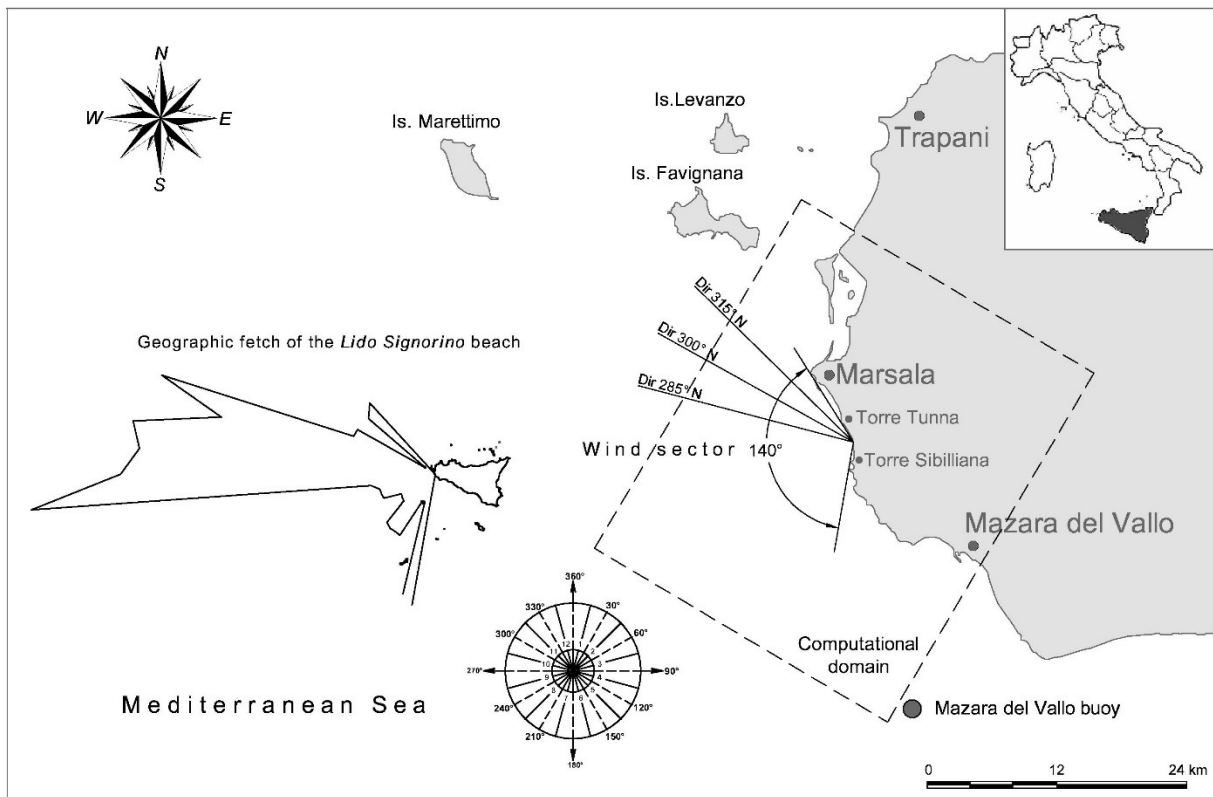


Fig. 2: Geographic location of Lido Signorino beach with fetch diagram, computational domain for wave propagation from offshore to inshore, main wave directions and location of the *Mazara del Vallo* buoy.

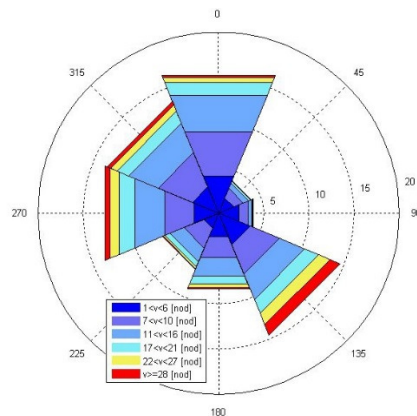


Fig. 3: Wind diagram obtained from measurements taken at Trapani meteorological station.

The beach stretch belongs geologically to the coastal plain known as that of *Marsala - Mazara del Vallo* (two towns close to the beach) which is oriented in the NW-SE direction and slopes gently towards the sea in the NE-SW direction. This zone is generally characterized by roughly constant and smooth morphological lineaments, which are typical of wide coastal plains modelled by sea action in the Quaternary period. The rocks cropping out are mainly Calcarenes constituted by carbonate sandy sediments, which settled further to a sea transgression in the middle Pleistocene. The beach is constituted by very fine Holocene sand with sub-rounded grains constituted by lithic and fossil shell fragments with a carbonate composition. The granulometric analysis gave a mean value of $D_{60} = 0.55$ mm and mean granulometric fractions of 0.4% of silt, 0.6% of clay and 99% of sand.

The dominant wind diagram (Fig. 3), obtained from measurements of the nearby meteorological station of Trapani in the period 2004-2008, shows that the winds which can mainly model the beach have NW-SE and W-E directions.

The intense coastal utilization for housing and economic activities produced buildings erected closer and closer to the swash zone (Fig. 1), causing progressive demolition of coastal dunes, which are a natural sand reservoir. The dunes, which in the 1950s were uniform from north to south and about 5 m high, are now discontinuous, concentrated in the southern part, where the population density is lower, and are on average 2.5 m high only.

The beach topographic survey, necessary for the subsequent processing, concerned the following: the dune scarp line, the berm above sea level and 26 transects (Fig. 4). For each transect, the slope was determined and then used for assessing the effects of wave motion and tide on the position of the instantaneous land-sea boundary. Although the beach profile changes with the seasons, due to the different wave motion energy, the general morphological characteristics, such as the slope, on average remain unchanged, so that the beach is *stable*

4 WAVE MOTION CHARACTERISTICS

In order for the effects of wave motion on the land-sea boundary fluctuations to be assessed the wavemeter data of the *Mazara del Vallo* buoy (DATAWELL Directional wavec MkI) were used, whose co-ordinates are $37^{\circ} 38' 43.19''$ N e $12^{\circ} 34' 57.0''$ E. The data, recorded every 3 hours, were the following: significant wave height, H_s [m], peak period, T_p [s], mean wave period, T_m [s], and mean wave direction, θ [$^{\circ}$ N], all related to the time interval between July 1st 1989 and April 4th 2008, during which, however, the buoy did not operate continuously. Examination of the data pointed out that, in the observation period, the Lido

Signorino beach was subject to 602 sea storms with the highest frequency along the 285° N direction.

Because of the different geographic position of the buoy and the beach, a geographic transposition of the data from the buoy to the area off the beach was performed. As the beach had relatively moderate fetches, the spectral significant wave height, H_s , and the spectral peak period, T_p , were expressed by the following well-known relationships (Vincent, 1984):

$$\frac{gH_s}{U_A^2} = 1.6 \cdot 10^{-3} \left(\frac{gF}{U_A^2} \right)^{1/2}; \quad \frac{gT_p}{U_A} = 2.857 \cdot 10^{-1} \left(\frac{gF}{U_A^2} \right)^{1/3} \quad (1)$$

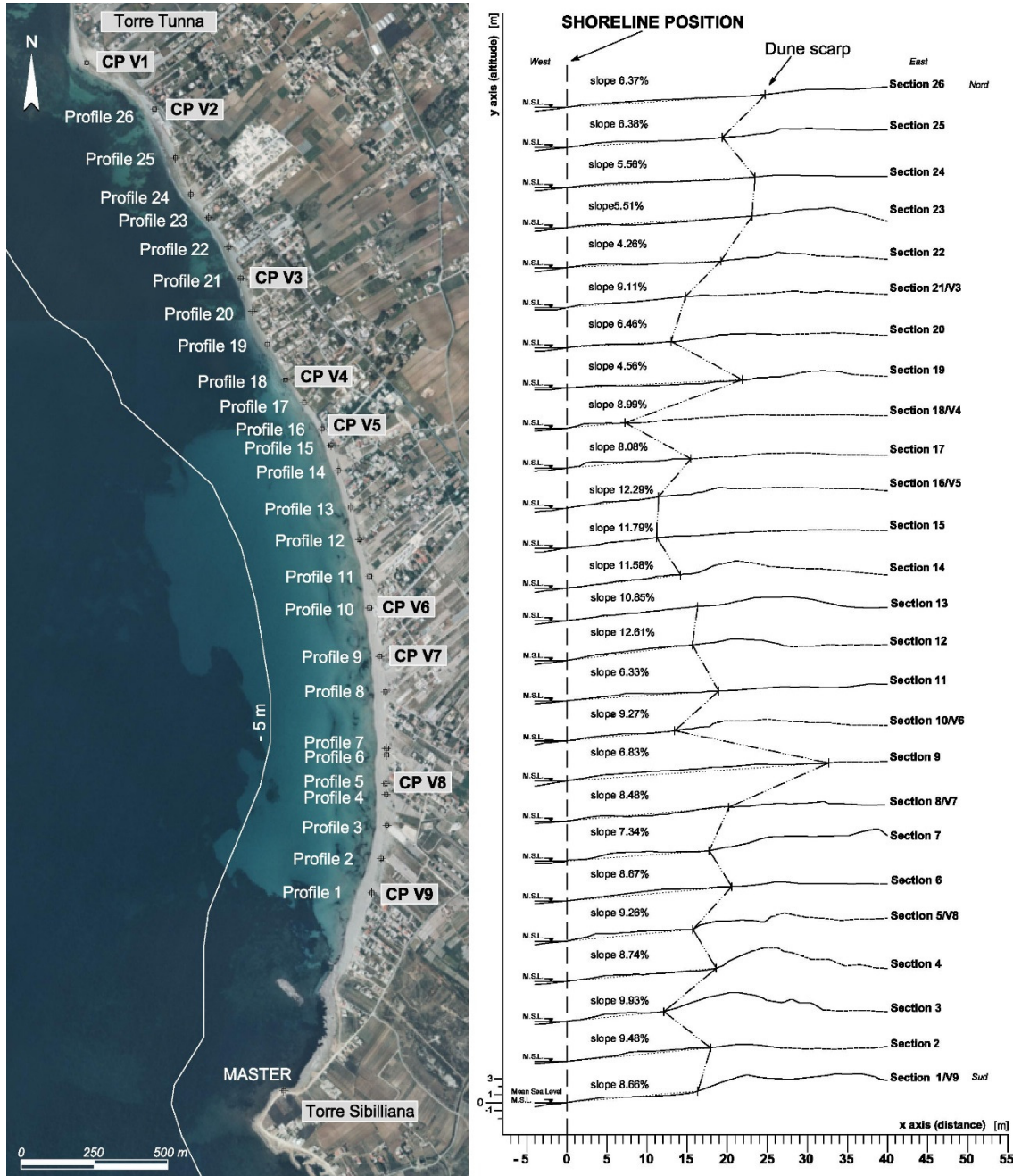


Fig. 4: Aerial images of the beach with 26 transects (left panel) and transect profiles (right panel); broken line indicates dune scarp.

where U_A is the wind velocity factor, depending in a non-linear way on the wind velocity measured at 10 m above sea level, and F is the effective fetch in the direction considered. Eqs. (1), written for the measurement point, O , and the transposition point, P , after obvious steps led to:

$$\frac{H_s^P}{H_s^O} = \left(\frac{F^P}{F^O} \right)^{1/2}; \quad \frac{T_p^P}{T_p^O} = \left(\frac{F^P}{F^O} \right)^{1/3} \quad (2)$$

Of course, the use of these expressions implied the wind velocity to be the same at both points, which is very likely in our case considering the buoy and beach positions.

The transposed wavemeter data were analysed statistically. The analysis was carried out both for the single measurements and for the whole sea storms. In both cases, the statistical analyses were both omni-directional and directional.

The analyses of the *single measurements* were performed in the domain of the significant wave heights $H_s > H_c = 1.5$ m adopting probability distributions of the Weibull type (Battjes 1974); the threshold $H_c = 1.5$ m was proposed by Boccotti (2000) for the Mediterranean Sea. For the *omni-directional* analysis, the empirical frequencies of exceedance (H_s higher than a generic observed height H) were used all together to achieve the parameters of the Weibull distribution describing the probability that H_s is higher than a fixed H value:

$$P(H) = \exp \left[- \left(\frac{H}{w} \right)^k \right] \quad (3)$$

where k and w are the distribution parameters. The probabilistic chart in Fig. 5, which in the abscissa and in the ordinate shows the variables, respectively, $X = 100 \ln(2.5H)$ and $Y = 100 \ln[\ln(1/P)]$, shows the good fitting of the points to the Weibull distribution in the range of H_s values between the critical threshold $H_c = 1.5$ m and about 5.8 m ($132 < X < 270$); for higher values the fitting is less satisfactory, which was predictable.

For the *directional* analysis, the probability to be looked for is that for which, for a fixed direction θ ($\theta_1 < \theta < \theta_2$), the height H_s exceeds a generic height H . This probability is expressed by:

$$P(H, \theta) = \exp \left[- \left(\frac{H}{w_\alpha} \right)^k \right] - \exp \left[- \left(\frac{H}{w_\beta} \right)^k \right] \quad (4)$$

where k is the same as in the omni-directional distribution, w_α and w_β are parameters depending on the sector (θ_1, θ_2) which were determined as proposed by Boccotti (2000). The good fitting of Eq. 4 to the points is shown once again in Fig. 5, which gives the curve related to the direction 285°N (Fig. 2), that of the most frequent sea storms; unlike the omni-directional probability, Eq. 4 is represented on this diagram by a curved line. Taking into account the expression of the Y variable, it is obvious that the directional probability curve is above the omni-directional probability straight line. The probability given by Eq. 4 allowed the return period to be calculated as follows:

$$T_r = \frac{1}{\lambda \cdot P(H)} \quad (5)$$

in which $\lambda = 2447$ is the mean number of observations in a year. For the most frequent sea storm direction 285°N , with the return period $T_r = 1$ year we obtained: $H_{s,T_r=1} = 5.62$ m from which $T_{p,T_r=1} = 10.1$ s.

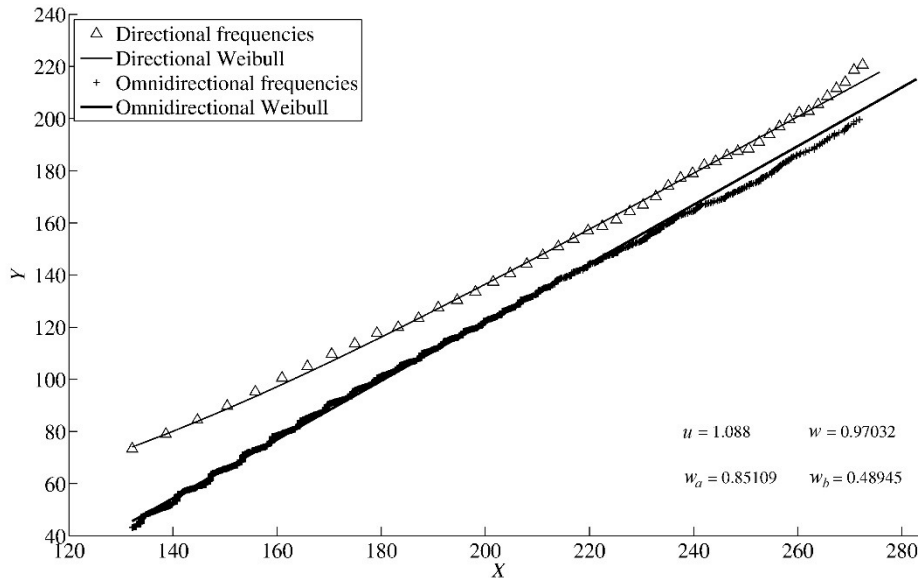


Figura 5: Comparison, in probabilistic chart, between the empirical frequencies of the measured H_s values and related Weibull distribution, both for omni-directional and directional (285°N) analysis.

in which $\lambda = 2447$ is the mean number of observations in a year. For the most frequent sea storm direction 285°N , with the return period $T_r = 1$ year we obtained: $H_{s,T_r=1} = 5.62$ m from which $T_{p,T_r=1} = 10.1$ s.

As for the analysis of *the whole storms*, we adopted the method of the *Equivalent Triangular Storm* (ETS method) proposed by Boccotti (2000), which will now be briefly recapitulated. The author assumes as a *single sea storm* a sequence of sea states during which the significant wave height, H_s , exceeds a fixed critical threshold, H_c , and does not drop below this threshold for a time interval higher than a fixed Δt_c . Boccotti himself proposes assuming $\Delta t_c = 12$ hours and, for the Mediterranean Sea, $H_c = 1.5$ m. Indeed, the ETS method allows considerable analytical simplification in the description of storm characteristics. In fact, actual storm time "histories", $H_s(t)$, are irregular and usually different from one storm to another, whereas for each storm the ETS method assumes a sea state varying with a *triangular law*.

The triangle height a (Fig. 6) is equal to the maximum significant height, $H_{s,max}$, of the actual storm, while the base b has to be determined so that the expected maximum height of the equivalent storm is equal to the expected maximum wave height of the actual storm. In the statistical analysis the method only considers the 10 most intense equivalent storms of each observation year. Indicating with a_{10} and b_{10} the mean values of a and b of the storms of each buoy (the subscript 10 refers to the number of storms considered for each year), the estimated duration value, \bar{b} , for the storm of intensity a , is given by the following linear regression:

$$\bar{b} = b_{10} \left(n - m \frac{a}{a_{10}} \right) \tag{6}$$

in which n and m are parameters to be determined empirically. According to Arena (1999), for Italian sea buoys the following mean values can be assumed: $n = 1.11$ and $m = 0.11$. The characteristics of each equivalent storm, a and b , are then processed statistically considering they are not independent of each other, by definition. The *directional* return period was determined by Arena (1999) who obtained the following expression:

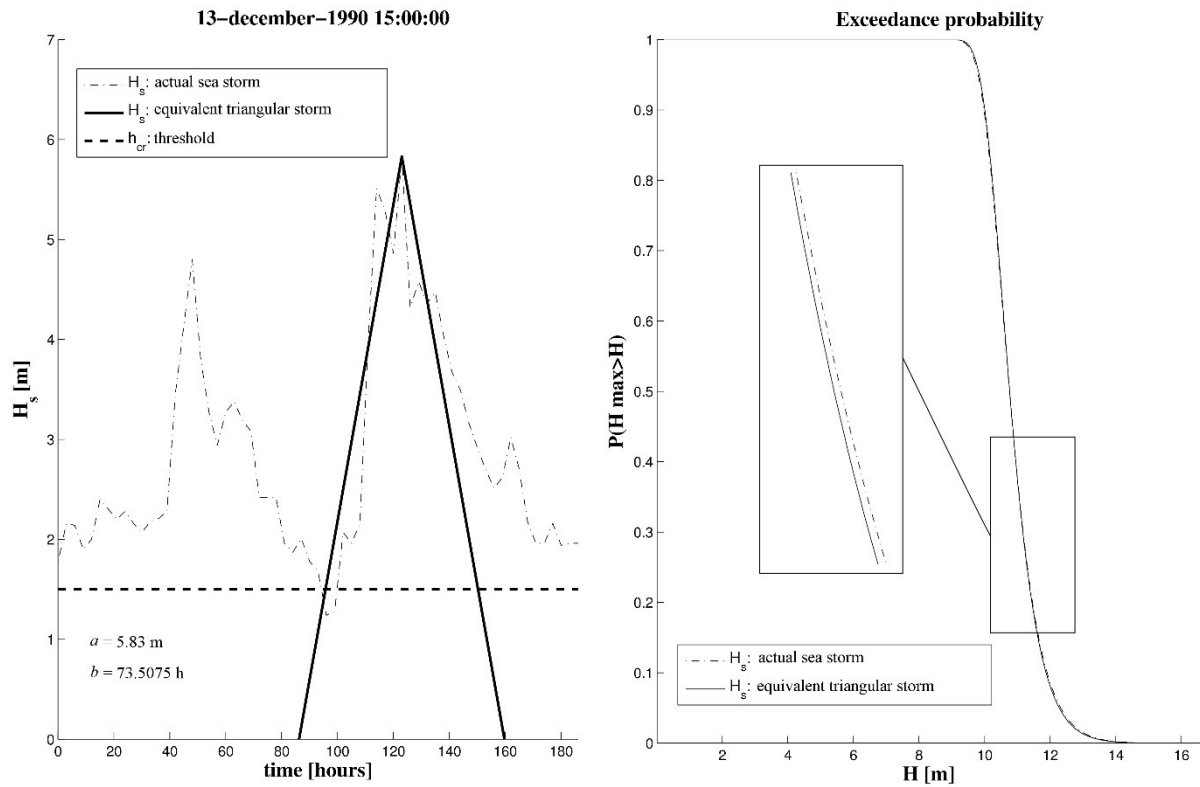


Fig 6: Triangular equivalent storm of an actual storm recorded at Mazara del Vallo buoy (left panel) and comparison between respective exceedance probability curves (right panel).

$$T_r(H, \theta) = \frac{\bar{b}(H)}{\lambda \cdot \left\{ \exp \left[- \left(\frac{H}{w_\alpha} \right)^k \right] \cdot \left[1 + k \left(\frac{H}{w_\alpha} \right)^k \right] - \exp \left[- \left(\frac{H}{w_\beta} \right)^k \right] \cdot \left[1 + k \left(\frac{H}{w_\beta} \right)^k \right] \right\}} \quad (7)$$

where the parameters w_α and w_β are the same as in Eq. 4 and, for a fixed H value ($\equiv a$), \bar{b} is given by Eq. 6.

With the data set of the Mazara del Vallo buoy transposed off the Lido Signorino beach we obtained $a_{10} = 4.5$ m and $b_{10} = 77$ h; then, for the return period $T_r = 1$ year and direction 285° N, Eq. 7 gave $H_{s,T_r=1} = 5.73$ m, from which $T_{p,T_r=1} = 10.2$ s, values very close to those obtained by direct processing of the observed significant heights. The practical coincidence of the results obtained by the two methods, on the one hand, strengthens the robustness of the latter method and, on the other hand, corroborates the accuracy of the results of both methods. In the following calculations we used the results of the ETS method.

After the offshore wave motion characteristics were known, the inshore ones were drawn up to a depth of 5 m using the spectral propagation model SWAN (*Simulating Waves Nearshore - Cycle III version 40.72*) by the Delft University of Technology (The Netherlands). We chose this model because of the reliability and robustness shown in many applications (e.g.: Boij et al., 1999; Holhijsen et al., 1993; Ris et al., 1999), its ease of employment and the fact that it is open-source. The computation domain (Fig. 2) was 36.4×30.5 km² with a square mesh having $\Delta x = \Delta y = 100$ m. The propagation results are shown in Fig. 7, in which the arrows indicate the direction of propagation and the significant

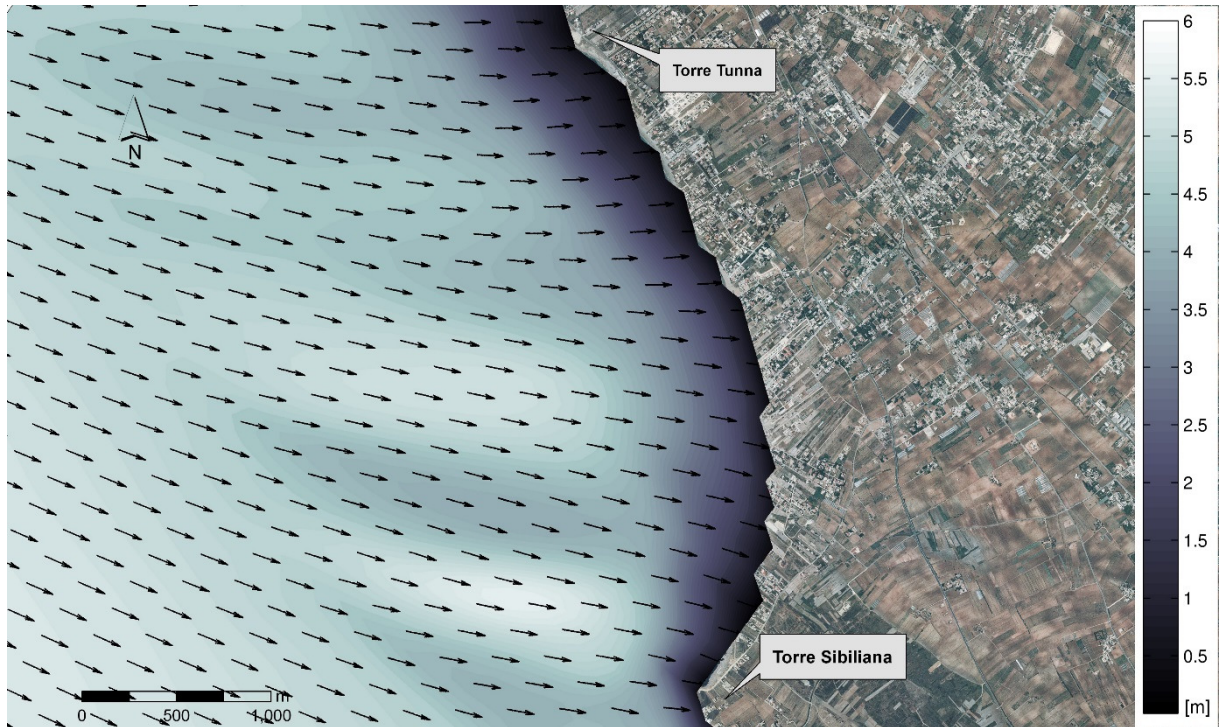


Fig 7: . Inshore waves obtained by SWAN model: arrows indicate wave directions and grey scale significant wave heights.

and the mean period proved to be $H_{s,60} = 5.32$ m and $T_{m,60} = 7.79$ s whereas at a wave height is represented through a colour scale. At a depth of 60 m the significant height depth of 5 m $H_{s,5} = 2.91$ m and $T_{m,5} = 7.27$.

5 RUN-UP AND RUN-DOWN EFFECTS

The inshore waves were used to calculate, in the 26 transects considered (Fig. 4), the wave motion effects on the instantaneous position of the land-sea boundary, *i.e.* the maximum and minimum level reached by the waves on the beach known as, respectively, the run-up and run-down (Stockdon, 2006). For this purpose, a physically based Lagrangian shoreline model for highly non-linear Boussinesq models was used and, for a comparison, the run-up was also assessed by an empirical formula.

5.1 Calculation of run-up and run-down by the numerical model

The numerical model is that proposed by *Lo Re et al.* (2012), which is integrated along the vertical and suited for breaking waves. The equations are solved in terms of the free surface elevation from the still level, ζ , and of the mean horizontal velocity along the depth, u . As introduction of the land-sea boundary condition in Boussinesq numerical models is rather involved, the land-sea boundary line position, located through its horizontal co-ordinate $\xi(t)$ (orthogonal to the shore), and the boundary line advance velocity u_b were calculated by solving the *lagrangian* equations of the boundary line movement. This gave:

$$\frac{d\xi}{dt} = u_b \quad (8)$$

which indicates that the fluid particles belonging to the boundary line remain on the line itself. The boundary line acceleration is given by (Prasad and Svendsen, 2003):

$$\frac{du_b}{dt} = -g \frac{\partial \zeta_b}{\partial x} \Big|_b + F_{fric} \quad (9)$$

where ζ_b is the surface elevation at the boundary line and F_{fric} the bottom friction term estimated by:

$$F_{fric} = -\frac{f}{h + \zeta} \cdot u \cdot |u| \quad (10)$$

where h is the local depth and f the friction factor. As, because of low depth, the term F_{fric} becomes too high, the model automatically contains its value which is then calculated by the simple relationship:

$$F_{fric} = -C_f \cdot u \cdot |u| \quad (11)$$

where C_f is a coefficient that, analogously to Lo Re et al. (2012), in the present paper was assumed equal to 5 m^{-1} .

The model was applied from the bathymetric 5 to the beach, simulating cnoidal breaking waves with the significant height given by the SWAN model. This choice is justified by our goal, which was not the simulation of a series of run-up and run-down random values but was assessment of their *significant* values only. For each transect, in the simulations a fictitious channel was considered having its main axis along the direction of wave propagation (orthogonal to the beach). From the bathymetric 5 to the beach the channel bottom was like the beach bottom, whereas off the bathymetric 5 a horizontal bottom 300 m long was assumed in order for stabilization of the waves imposed in the initial cross section to be obtained. The computation domain was discretized by intervals $\Delta x = 1 \text{ m}$ and $\Delta t = 0.00727 \text{ s}$; the simulations concerned 50 waves in input with a Courant number equal to 0.047. Fig. 8 shows, as an example, the simulation for transect 8, for which the input at the bathymetric 5 were: $H_s = 2.91 \text{ m}$ and $T = 7.27 \text{ s}$. The panels in the figure show a brief sequence of the simulated run-up: *a*) situation before the breaking; *b*) breaking start (the area between the unbroken and the dashed lines is the roller); *c*) and *d*) wave advance after breaking.

The *horizontal* run-up and run-down values obtained for all the 26 transects are shown in Tab. 1, which shows that the horizontal run-up ranges between about 7 and 20 m respectively for the maximum and the minimum beach slope, while the horizontal run-down stabilizes at about 10 cm only, with maximum and minimum absolute values respectively for the minimum and the maximum beach slope.

5.2 Calculation of the run-up by an empirical formula

For a comparison, run-up was also calculated by the empirical formula of Nielsen & Hanslow (1991), which was chosen among the others (*e.g.*, Holman and Sallenger, 1985; Raubenheimer and Guza, 1996; Hughes, 2004) as it was obtained for beaches having geomorphologic and granulometric characteristics analogous to ours. The authors took measurements on six beaches in New South Wales in Australia. The beaches were constituted by fine sands with a mean diameter between 0.4 and 0.22 mm; the offshore wave parameters were taken by a buoy located 30 km from the coast. Nielsen and Hanslow found that run-up is given by:

$$R = 0.89 \cdot L_{zwm} \quad (12)$$

where L_{zwm} is the vertical scale of the Rayleigh distribution followed by the experimental run-up values, *i.e.* the shape parameter of the distribution itself, which according to the authors is given by:

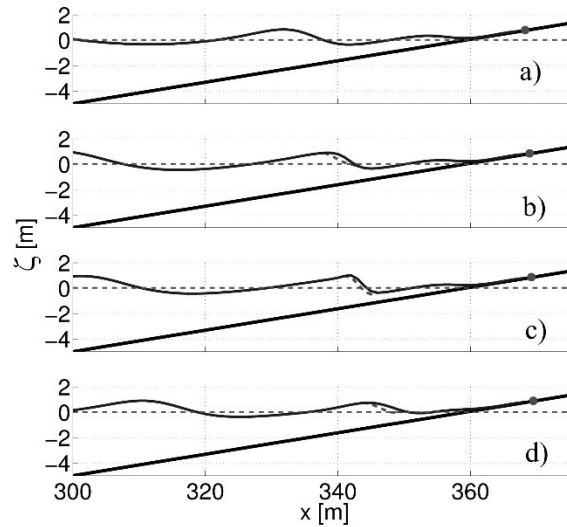


Fig 8: Stages of simulated run-up in transect 8 (slope 8.48%): a) wave before breaking; b) wave at incipient breaking; c) wave breaking; d) wave maximum run-up.

Transect	Beach slope	Numerical model		Empirical formula
		Horizontal run-up [m]	Horizontal run-down [m]	Horizontal run-up [m]
1	8.66 %	10.04	-0.10	9.69
2	9.48 %	8.77	-0.11	8.46
3	9.93 %	8.76	-0.11	8.45
4	8.74 %	9.95	-0.10	9.60
5	9.26 %	9.4	-0.10	9.07
6	8.67 %	10.03	-0.10	9.68
7	7.34 %	11.86	-0.09	11.44
8	8.48 %	10.26	-0.10	9.90
9	6.83 %	12.74	-0.09	12.29
10	9.27 %	9.34	-0.11	9.06
11	6.33 %	13.74	-0.08	13.26
12	12.61 %	6.9	-0.12	6.66
13	10.85 %	8.02	-0.11	7.74
14	11.58 %	7.51	-0.12	7.25
15	11.79 %	7.38	-0.12	7.12
16	12.29 %	7.08	-0.12	6.83
17	8.08 %	10.77	-0.10	10.39
18	8.99 %	9.68	-0.10	9.34
19	4.56 %	19.08	-0.05	18.41
20	6.46 %	13.46	-0.08	12.99
21	9.11 %	9.54	-0.10	9.21
22	4.26 %	20.43	-0.04	19.71
23	5.51 %	15.79	-0.07	15.24
24	5.56 %	15.65	-0.07	15.10
25	6.38 %	13.64	-0.08	13.16
26	6.37 %	13.66	-0.08	13.18

Tab. 1: Run-up and run-down values obtained by the numerical Boussinesq model and run-up values given by the Nielsen & Hanslow empirical formula.

$$L_{zwm} = \begin{cases} 0.60 \cdot (H_{0rms} \cdot L_0)^{0.5} \tan\gamma & \text{for } \tan\gamma > 0.10 \\ 0.05 \cdot (H_{0rms} \cdot L_0)^{0.5} & \text{for } \tan\gamma \leq 0.10 \end{cases} \quad (13)$$

where $H_{0rms} = 0.706 \cdot H_s$ is the mean square value of the offshore wave heights, $L_0 = gT^2/2\pi$ the offshore wave length and $\tan\gamma$ the beach slope.

The R values obtained by us for the Lido Signorino beach, taking into account the profiles in Fig. 4, yielded the horizontal run-ups reported in Tab. 1, which shows analogous values to those of the mathematical model.

6 TIDE EFFECTS

Advancing and retreating of the instantaneous land-sea boundary caused by tides were estimated by processing the fluctuations gauged by the closest tide gauge, located at Porto Empedocle halfway along the southern Sicilian coast. The measurements were hourly and taken in the period 1999-2009. Fig. 9 shows, as an example, the 2005 records. In each year tide fluctuations are noticeably variable, as they do not depend on astronomic contributions only but also on meteorological ones (Tomaselli *et al.*, 2011). The records show several peaks that are considerably higher than the measurements at hours close to one another: such peaks are probably gauging errors (spikes). In order for a reliable fluctuation range to be recognized, as a comparison term, the *astronomic* tide was first determined. The latter was yielded, year by year, by a data harmonic analysis using the *T_TIDE* code (Pawlowicz *et al.*, 2002) which operates in the *MatLab* environment. Fig. 9 also reports the 2005 astronomic tide; in the figure, the mean sea level and the 1-year period harmonic due to Earth revolution around the Sun are highlighted. Examination of the figure shows that the astronomic tide ranges in a strip about 25 cm wide and that the gauged tide sometimes reaches considerably higher values than the astronomic tide. The difference between the gauged tide and the astronomic tide, known

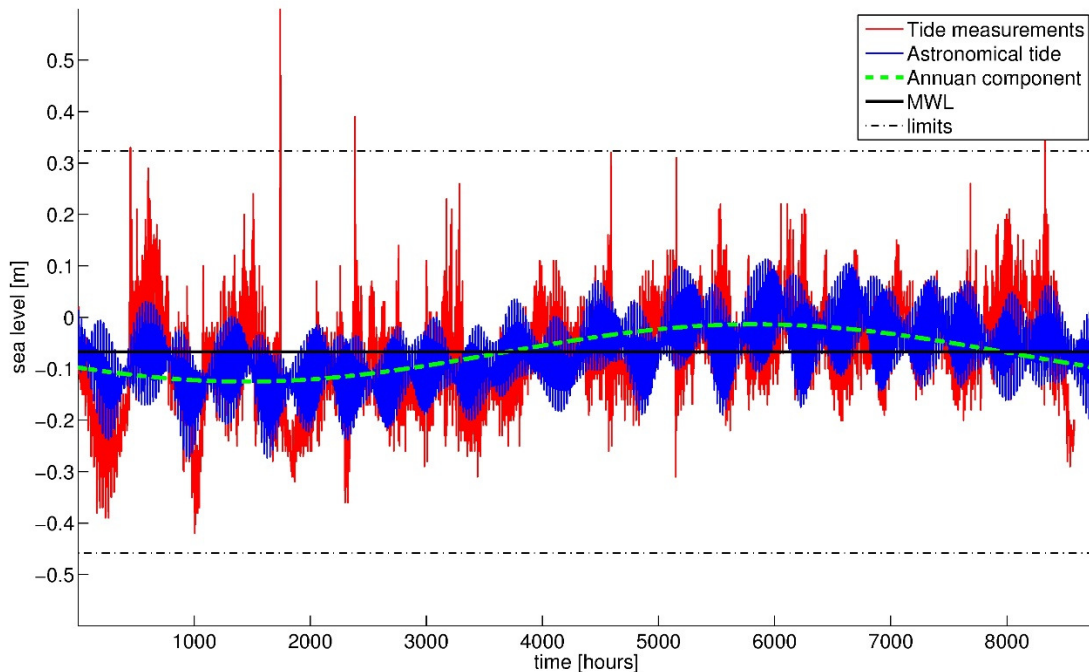


Fig 9: Tide fluctuations recorded at *Porto Empedocle* station; the figure also reports astronomic tide yielded by data harmonic analysis and yearly harmonic.

as residual or noise, is the contribution due to the various meteorological factors (atmospheric pressure, storm surge, *etc.*) (Pawlowicz *et al.*, 2002; Tomaselli *et al.*, 2011). In order for the extreme and unlikely peaks to be excluded from the present analysis, for each year, measurements were discarded if falling outside the strip around the mean sea level having width equal to 8 times the standard deviation of all the tide measurements. The remaining measurements were used to assess the highest land-sea boundary shifts due to tide fluctuations. For this purpose the mean of the highest yearly tide levels and the mean of the lowest yearly tide levels were calculated, which respectively proved to be 0.402 m and -0.405 m with respect to the mean sea level.

7 UNCERTAINTIES IN LOCATING THE SHORELINE

As the highest wave and tide effects on the land-sea boundary movement were determined, it was possible to bound, starting from instantaneous images of the boundary itself, a strip within which the shoreline *had to fall*. In what follows it was assumed that the shoreline was the boundary related to the *mean sea level*; the adjustments to the proposed method for a different choice (*e.g.*, the mean of the high tides) are obvious. In order to locate the strip bounds, it has to be noted that, for each transect, the position P_i of the instantaneous boundary shown by the images can only fluctuate within the range:

$$\Lambda - RD - MD \leq P_i \leq \Lambda + RU + MU \quad (14)$$

where Λ is the shoreline position, RU the horizontal run-up, RD the horizontal run-down, MU the boundary advance due to the maximum tide level and MD the retreat due to the minimum tide level. From Eq. 14 we obtain:

$$P_i - RU - MU \leq \Lambda \leq P_i + RD + MD \quad (15)$$

which allows one to bound the strip around P_i within which the shoreline has to fall (Fig. 10). As this strip contains all the positions the boundary can take on, even the two extreme ones, its width gives the *maximum error*, for ordinary sea storms, that we could make when assuming the shoreline as coincident with the land-sea boundary fixed in the images. This strip, in short, is an *uncertainty band*.

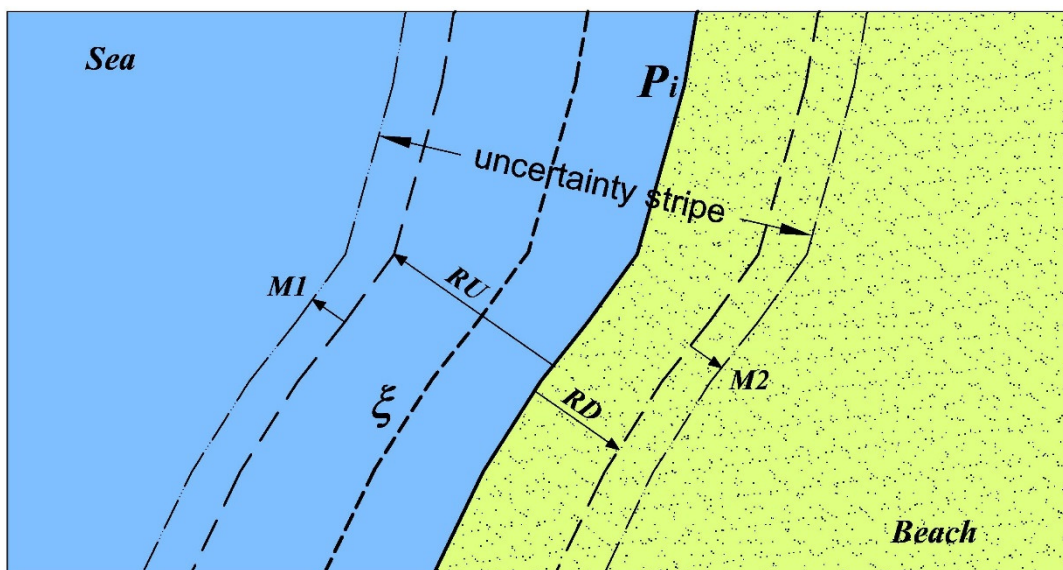


Fig 10: Determination of uncertainty strip around instantaneous land-sea boundary line.

Transect	Beach slope	Uncertainty band width [m]
1	8,66 %	19,18
2	9,48 %	17,11
3	9,93 %	16,71
4	8,74 %	19,00
5	9,26 %	17,93
6	8,67 %	19,16
7	7,34 %	22,67
8	8,48 %	19,59
9	6,83 %	24,37
10	9,27 %	17,86
11	6,33 %	26,30
12	12,61 %	13,13
13	10,85 %	15,28
14	11,58 %	14,30
15	11,79 %	14,05
16	12,29 %	13,47
17	8,08 %	20,58
18	8,99 %	18,47
19	4,56 %	36,59
20	6,46 %	25,76
21	9,11 %	18,21
22	4,26 %	39,16
23	5,51 %	28,74
24	5,56 %	29,97
25	6,38 %	26,11
26	6,37 %	26,14

Tab. 2: Uncertainty strip width in the 26 transects..

Application of the method to the Lido Signorino study case, with the data obtained in the previous sections, led us to assess the strip widths reported in Tab. 2. The latter shows that the uncertainty strip width ranged between about 13 and 40 m, with a mean of about 22 m. Such high values of the errors that we risk making, although an unexceptional sea storm and a moderate tide range were taken into account, advise us to be prudent in jumping to conclusions on the shoreline position by aerial imagery analysis only. By contrast, imagery analysis has to be interpreted in the light of in-depth geomorphologic and hydraulic-maritime studies, better still if they are contextualized with the meteorological-marine and astronomic conditions at shooting time.

The uncertainty strip width, moreover, sets serious limits in studying littoral evolution by the use of images only. Littoral evolution, in fact, occurs with advances and retreats being, usually, of a few metres per year at the most, *i.e.*, a considerably smaller amount than the error we risk making in shoreline assessment for a given year.

8 CONCLUSIONS

The topic of shoreline location was addressed, a topic of considerable practical interest both for settlement of dispute between the state and private citizens on state property boundaries and for productive activity planning (*e.g.*, concession issues) and for coastal management (*e.g.*, designing of coastal protection works). It was recognized that the

intrinsically dynamic nature of the land-sea boundary, continually variable because of endless fluctuation in the sea surface due to tide, currents and wave motion, and the consequent coastal modelling, makes it necessary to adopt some criteria to choose which, among the countless instantaneous locations of the land-sea boundary, we can assume as the shoreline.

This uncertainty is mirrored by the rules of the various coastal states which define the shoreline in different ways. However, whatever criterion is chosen, the practical problem of studying suitable techniques for its location remains to be solved.

Examination of the technical literature showed that shoreline location is more and more often obtained by remote sensing imagery analysis, using different techniques each having advantages and disadvantages with respect to the others. Actually, there are not many methods coupling imagery analysis and beach geomorphologic factors (of beach above and below sea level), wave motion, tides and sediment transport, which are error sources in shoreline location. Such errors were assessed in the present study, considering the particular case of a steady beach on the Mediterranean Sea, subject to moderate tide and "ordinary" wave motion.

The beach geomorphologic survey allowed the characteristic morphotypes to be recognized, whereas the topographic survey allowed 26 transects to be drawn for the subsequent hydraulic maritime study.

Wave motion effects were assessed using wavemetric data of a nearby buoy, which were transposed to off the waters using formulas taken from the technical literature. The transposed data were then processed statistically in order to obtain the characteristics of a 1-year return period storm, assumed as the maximum of the "ordinary" sea storms. The statistical analysis was carried out both directly processing the single wave significant heights and processing the characteristics of the whole sea storms, through the concept of *equivalent triangular storm* (ETS method). The two analyses gave analogous results, thus corroborating each other. The offshore wave parameters were then propagated up to shallow waters, by the known spectral model SWAN, and were used for run-up and run-down calculation. Run-up and run-down were calculated on every transect by the use of a numerical Boussinesq model which uses a Lagrangian type boundary condition. For a comparison, run-up was also calculated using a well-known empirical formula that gave not very different results.

In order to assess tide fluctuation effects the measurements recorded in the closest tide gauge were processed, considering both the astronomic and the meteorological tide. The reliability of each measurement was assessed by comparison with the astronomic tide, obtained by harmonic analysis of the measurements using the T_TIDE software.

Finally, cumulating wave and tide effects allowed us to recognize that the instantaneous land-sea boundary can range within a strip that, in the specific geomorphologic and hydraulic-maritime beach conditions, is even a few dozen metres wide. The shoreline must fall within this strip, which, therefore, gives the maximum error we could make whenever we assume the shoreline as coincident with the land-sea boundary line fixed in remote imagery.

Such wideness of the uncertainty strip, although a not extraordinary sea storm and a moderate tide were considered, warns us to be prudent when assuming as the shoreline that identified by aerial imagery only. By contrast, imagery analysis has to be interpreted in the light of in-depth geomorphologic and hydraulic-maritime studies, better still if they are contextualized with meteorological-marine and astronomic conditions at shooting time.

These noticeable uncertainties recognized for shoreline location by imagery analysis only affect the reliability of coastal evolution studies carried out using images, as annual shoreline advances and retreats are, usually, a few orders of magnitude lower than the possible error for one year.

In conclusion, the present paper demonstrated the necessary for an interdisciplinary method to be applied for assessing a reliable shoreline location, which accounts for the peculiar beach characteristics. This important topic has to be further examined considering beaches having different geomorphologic characteristics and subject to more severe meteorological-marine conditions.

ACKNOWLEDGMENTS

The writers thank the Istituto Idrografico della Marina Militare Italiana (Hydrographic Institute of the Italian Navy) which gave them the bathymetric data used in the paper.

SYMBOLS

a	Maximum wave height of an equivalent sea storm
a_{10}	Mean of the highest 10 a values of each observation year
b	Duration of the equivalent sea storm having intensity a
\bar{b}	Estimated duration value of the sea storm having intensity a
b_{10}	Mean of the b values of the most intense 10 equivalent sea storms of each observation year
C_f	Friction coefficient for calculation of the F_{fric} term for low depths
D_{60}	Grain diameter related to 60% passing
f	Friction factor
F	Effective fetch
F^O, F^P	Effective fetch respectively at the buoy and the transposition point
F_{fric}	Friction term
g	Gravity acceleration
h	Local depth
H, H_s	Significant wave height
H_c	Critical threshold for the significant wave height
$H_{s,T_r=1}$	Significant wave height having a 1-year return period
$H_{s,5}, H_{s,60}$	Significant wave heights at the depths of, respectively, 5 and 60 m
H_s^O, H_s^P	Significant wave height at the buoy and the transposition point, respectively
H_{0rms}	Root mean square value of offshore wave heights
k, w, w_α, w_β	Weibull distribution parameters
L_0	Deep water wave length
L_{zwm}	Vertical scale of the run-up Rayleigh distribution
m, n	Parameters of linear regression for assessing \bar{b}
P_i	Instantaneous position of the land-sea boundary line
$P(H)$	Omni-directional probability for H_s to be higher than a fixed H value
$P(H, \theta)$	Directional probability for H_s to be higher than a fixed H value for a given direction θ
R	Run-up
RD	Horizontal run-down
RU	Horizontal run-up
T	Wave period
T_m	Mean wave period
T_r	Return period
T_p	Peak wave period
$T_{p,T_r=1}$	Peak wave period for a 1-year return period
$T_{m,5}, T_{m,60}$	T_m values at depths of, respectively, 5 and 60 m
T_p^O, T_p^P	Peak wave period at the buoy and the transposition point, respectively
$\tan \gamma$	Beach slope
u	Horizontal velocity averaged along the vertical

u_b	Advance velocity of the land-sea boundary line
U_A	Wind velocity factor
$X e Y$	Auxiliary variables
ζ	Free surface elevation with respect to the still level
ζ_b	Surface elevation at the boundary line
θ	Wave motion direction
λ	Mean number of yearly observations processed
Λ	Shoreline horizontal coordinate
ξ	Land-sea boundary line horizontal coordinate

REFERENCES

- Addo, A.K., Walkden, M., Mills, J.P., 2008. Detection, measurement and prediction of shoreline recession in Accra, Ghana. *ISPRS Journal of Photogrammetry and Remote Sensing*, Vol. 63, pp. 543-558.
- Archetti, R., Romagnoli, C., 2011. Analysis of the effects of different storm events on shoreline dynamics of an artificially embayed beach. In *Earth Surface Processes And Landforms*, Vol. 36, pp. 1449-1463.
- Arena, F., Barbaro, G. 1999. *Il rischio ondososo nei mari italiani*, Editoriale Bios, Cosenza.
- Baghdadi, N., Gratiot, N., Lefebvre, J.P., Oliveros, C., Bourguignon, A., 2004. Coastline and mud-bank monitoring in French Guiana: contributions of radar and optical satellite imagery. In *Canadian Journal of Remote Sensing*, Vol. 30(2), pp. 109-122.
- Battjes, J.A., 1974. Surf similarity, in 14th Coast Engrg. Conf., Vol. 20, pp. 257-293.
- Boak, E.H., Turner, L., 2005. Shoreline definition and detection: a review. In *Journal of Coastal Research*, Vol. 21(4), pp. 688-703.
- Boccotti, P., 2000. *Wave mechanics for ocean engineering*. Elsevier Science.
- Chen, W.W., Chang, H.K., 2009. Estimation of shoreline position and change from satellite images. In *Estuarine, Coastal and Shelf Science*, Vol. 84(1), pp.54-60.
- De Vries, S., Hill, D.F., De Schipper, M.A., Stive, M.J.F., 2011. Remote sensing of surf zone waves using stereo imaging. In *Coastal Engineering*, Vol. 58, pp. 239-250.
- Deronde, B., Houthuys, R., Debrun, W., Fransaeer, D., Van Lancker, V., Henriët, J.P., 2006. Use of airborne hyperspectral data and laserscan data to study beach morphodynamics along the Belgian coast. In *Journal of Coastal Research*, Vol. 22, pp. 1108-1117.
- Dolan, R., Hayden, B.P., May, P., May, S., 1980. The reliability of shoreline change measurements from aerial photographs. In *Shore and Beach*, Vol. 48(4), pp. 22-29.
- Douglas, B.C., Crowell, M., 2000. Long-term shoreline position prediction and error propagation. In *Journal of Coastal Research*, vol.16, pp. 145-152.
- Hanson, H. Kraus, N., 1989. GENESIS: Generalized model for simulating shoreline change Technique Report CERC, pp. 89-19.
- Holman, R.A., Sallenger, A.H., Jr. 1985. Setup and swash on a natural beach, *Journal Geophysics Research*, 90(C1), 945-953.
- Hughes, S.A. 2004. Estimation of wave run-up on smooth, impermeable slopes using the wave momentum flux parameter, *Coastal Engineering*, 51(11-12),1085-1104.
- Komar, P.D., 1998. *Beach Processes and Sedimentation*. Upper Saddle River, New Jersey: Prentice Hall Inc., p. 544.
- Leatherman, S.P., 2001. Chapter 8 Social and economic costs of sea level rise. In Douglas, B.C., Kearney, M.S. and Leatherman, S.P., (eds.). *Sea level rise history and consequences*. San Diego California: Accademic Press., pp.232.

- Lee, D.S., Shan, J., 2003. Combining Lidar elevation data and IKONOS multispectral imagery for coastal classification mapping. In *Marine Geodesy*, Vol. 26, pp. 117-127.
- Lee, J.S., Jurkevich, I., 1990. Coastline detection and tracing in SAR images. IEEE. In *Transactions on Geoscience and Remote Sensing*, Vol. 28, pp. 662-668.
- Liu, H., Sherman, D., Gu, S., 2007. Automated extraction of shorelines from airborne light detection and ranging data and accuracy assessment based on Monte Carlo simulation. In *Journal of Coastal Research*, Vol. 23, pp. 1359-1369.
- Lo Re, C., Musumeci, R.E., Foti, E., 2012. A shoreline boundary condition for a highly nonlinear Boussinesq model for breaking waves, *Coastal Engineering*. Vol. 60(1) pp. 41-52
- Maiti, S., Bhattacharya, A.K., 2009. Shoreline change analysis and its application to prediction: A remote sensing and statistics based approach. In *Marine Geology*, Vol. 257, pp. 11-23.
- May, S.K.; Kimball, W.H.; Grady, N., Dolan, R., 1982. CEIS: The Coastal Erosion Information System. In *Shore and Beach*, Vol. 50, pp. 19-26.
- Morton, R.A., Speed, F.M., 1998. Evaluation of shorelines and legal boundaries controlled by water levels on sandy beaches. In *Journal of Coastal Research*, Vol. 14(4), pp. 1373-1384.
- Nielsen, P., Hanslow, D.J., 1991. Wave run-up distributions on natural beaches. In *Journal of Coastal Research*, Vol. 7, pp. 1139-1152.
- Parker, B.B., 2003. The Difficulties in Measuring a Consistently Defined Shoreline-the Problem of Vertical Referencing. In *Journal of Coastal Research*, Vol. 2003, pp. 44-56.
- Pawlowicz, R., Beardsley, B., Lentz, S., 2002. Classical tidal harmonic analysis including error estimates in MATLAB using T_TIDE. In *Computers & Geosciences*, Vol. 28, pp. 929-937.
- Prasad, R.S., Svendsen, I.A., 2003. Moving shoreline boundary condition for nearshore models. In *Coastal Engineering*, Vol. 49(4), pp. 239-261.
- Raubenheimer, B., Guza, R.T., 1996. Observations and predictions of run-up, *Journal Geophysics Research*, 101(C10), 25575-25587.
- Ris, R.C., Booij, N. Holthuijsen, L.H., 1999. A third generation wave model for coastal regions, part II: verification. In *Journal of Geophysical Research*, Vol. 104(4), pp. 7649-7666.
- Ruggiero, P., Komar, P.D., McDougal, W.G., Marra, J.J., Beach, R.A., 2001. Wave run-up, extreme water levels and the erosion of properties backing beaches. In *Journal of Coastal Research*, Vol. 17(2), pp. 407-419.
- Seymour, R., Guza, R.T., O'Reily, W., Elgar, S., 2005. Rapid erosion of a small southern California beach fill. In *Coastal Engineering*, Vol. 52, pp. 151-158.
- Shoshany, M., Degani, A., 1992. Shoreline detection by digital image processing of aerial photography. In *Journal of Coastal Research*, Vol. 8(1), pp. 29-34.
- Smith, A.W.S., Jackson, L.A., 1992. The variability in width of the visible beach. In *Shore and Beach*, Vol. 60(2), pp. 7-14.
- Stockdon, H.F., Holman R.A., Howd P.A., 2006. Sallenger Jr A.H. Empirical parameterization of setup, swash and run-up. In *Coastal Engineering*, Vol. 53(7), pp. 573-588.
- Tomaselli P.D., Lo Re C. , Ferreri G. B. 2011. Analysis of tide measurements in a Sicilian harbour. Proc. of the 5th International Short Conference On Applied Coastal Research - 5th SCACR, Shaker Verlag, RWTH Aachen University, Aachen, Germany, pp. 579-586.
- U.S. Army Corps of Engineers. 2008. Coastal Engineering Manual. Engineer Manual 1110-2-1100, U.S. Army Corps of Engineers, Washington, D.C. (in 6 volumes).

- Valpreda, E., Simeoni, U., 2003. Assessment of coastal erosion susceptibility at the national scale: the Italian case. In *Journal of Coastal Conservation*, Vol. 9, pp. 43-48.
- Zarillo, G.A., Kelley, J., Larson, V., 2008. A GIS Based Tool for Extracting Shoreline Positions from Aerial Imagery (Beach Tools) Revised. In *Coastal and Hydraulics Engineering Technical Note CHETN IV-37*, US Army Engineer Research and Development Center, Vicksburg, MS, Vol. 12, pp. 1-14.